

Energy Redistribution following CO₂ Formation on Cold Amorphous Solid Water

Meenu Upadhyay and Markus Meuwly*

*Department of Chemistry, University of Basel, Klingelbergstrasse 80 , CH-4056 Basel,
Switzerland.*

E-mail: m.meuwly@unibas.ch

December 2, 2021

Abstract

The formation of molecules in and on amorphous solid water (ASW) as it occurs in interstellar space releases appreciable amounts of energy that need to be dissipated to the environment. Here, energy transfer between CO_2 formed within and on the surface of amorphous solid water (ASW) and the surrounding water is studied. Following $\text{CO}(^1\Sigma^+) + \text{O}(^1\text{D})$ recombination the average translational and internal energy of the water molecules increases on the ~ 10 ps time scale by 15 % to 20 % depending on whether the reaction takes place on the surface or in an internal cavity of ASW. Due to tight coupling between CO_2 and the surrounding water molecules the internal energy exhibits a peak at early times which is present for recombination on the surface but absent for the process inside ASW. Energy transfer to the water molecules is characterized by a rapid ~ 10 ps and a considerably slower ~ 1 ns component. Within 50 ps a mostly uniform temperature increase of the ASW across the entire surface is found. The results suggest that energy transfer between a molecule formed on and within ASW is efficient and helps to stabilize the products generated.

1 Introduction

The motion of adsorbates in and on amorphous solid water (ASW) is essential for chemistry at astrophysical conditions. Typically, bulk water is present in the form of ASW which is the main component of interstellar ices.¹ The structure of ASW is usually probed by spectroscopic measurements^{1,2} although interference-based methods have also been employed.³ ASWs are porous structures characterized by surface roughness and internal cavities of different sizes which can retain molecular or atomic guests.⁴ Under laboratory conditions the water ices seem to be amorphous⁵ whereas the morphology of ices in the interstellar medium are more debated.⁶

The high porosity of ASW⁷⁻⁹ makes it a good catalyst for gas-surface reactions involving oxygen,¹⁰⁻¹⁶ hydrogen,¹⁷ carbonaceous^{18,19} and nitrogen-containing²⁰ species and helps maintaining those species on or inside ASW.^{21,22} This increases the probability for the reaction partners to diffuse to locations for collisions and association reactions to occur. As the diffusivity of individual atoms and small molecules has been established from both, experiments and simulations,^{15,23,24} this is a likely scenario for formation of molecules on and within ASW.

As such association reactions are in general exothermic, the energy released needs to be transferred to environmental degrees of freedom for the reaction products to stabilize. This is the quest of the present work which investigates the time scale and degrees of freedom to receive the energy liberated in the $O(^1D)+CO(^1\Sigma^+)$ reaction to form ground state $CO_2(^1\Sigma_g^+)$. The chemical precursors for formation of CO_2 are believed to be carbon monoxide and atomic oxygen and the $CO+O$ reaction has been proposed as a non-energetic pathway, close to conditions in interstellar environments, for CO_2 formation 20 years ago.²⁵ Formation of $CO_2(^1\Sigma_g^+)$ from ground state $CO(^1\Sigma^+)$ and electronically excited $O(^1D)$ is barrierless. The excited atomic oxygen species can, for example, be generated from photolysis of H_2O ²⁶ which has a radiative lifetime of 110 minutes.²⁷

Earlier thermoluminescence experiments suggested that the $O(^3P)+CO(^1\Sigma^+)$ reaction with both reaction partners in their electronic ground state yields excited CO_2^* which, after emission of a photon, leads to formation of CO_2 .²⁸ Such a process has also been proposed to occur on interstellar grains²⁹ and has been confirmed experimentally²³ with an estimated entrance barrier of 0.014 eV to 0.103 eV for the process on ASW, compared with a value of 0.3 eV from high-level electronic structure calculations.³⁰ The surrounding water matrix provides the necessary coupling²⁵ to facilitate relaxation of the $^3A'$ or $^3A''$ states of CO_2 to the $^1A'$ ground state (correlating with linear $^1\Sigma_g^+$).

For adsorbed species to react on ASW they need to be able to diffuse. This has been demonstrated from MD simulations with diffusion coefficients and desorption energies consistent with experiments.^{24,31} Atomic oxygen¹⁵ on ASW experiences diffusional barriers between $E_{\text{dif}} = 0.2$ kcal/mol and 2 kcal/mol (100 K to 1000 K) compared with values of $E_{\text{dif}} = 990_{-360}^{+530}$ K determined from experiments.²¹ For CO, MD simulations reported¹⁶ desorption energies between 3.1 and 4.0 kcal/mol (1560 K to 2012 K or 130 meV to 170 meV), compared with 120 meV from experiments. On non-porous and crystalline water surfaces submonolayer desorption energies for CO are 1307 K and 1330 K (~ 115 meV), respectively.³²

After recombination $\text{O}(^1\text{D}) + \text{CO}(^1\Sigma^+) \rightarrow \text{CO}_2(^1\Sigma_g^+)$ the product is in a highly vibrationally excited state. For it to stabilize, excess internal energy needs to be channeled into the environment which is the ASW. The present work characterizes and quantifies energy relaxation of the $\text{CO}_2(^1\Sigma_g^+)$ product into internal and translational degrees of freedom of the surrounding water matrix. First, the methods used are described. Then, results are presented and discussed. Finally, conclusions are drawn.

2 Computational Methods

All molecular dynamics (MD) simulations were carried out using the CHARMM suite of programs³³ with provisions for bond forming reactions through multi state adiabatic reactive MD (MS-ARMD).³⁴ The simulation system, see Figure 1, consisted of an equilibrated cubic box of amorphous solid water with dimension $31 \times 31 \times 31 \text{ \AA}^3$ containing 1000 water molecules. As all bonds and angles are flexible, the simulations were run with a time step of $\Delta t = 0.1$ fs and the non-bonded cutoff was at 13 \AA . Simulations were started from an existing, equilibrated ASW structure^{15,16,35} by adding CO_A and O_B inside (Figure 1A) or on

top of (Figure 1B) ASW.

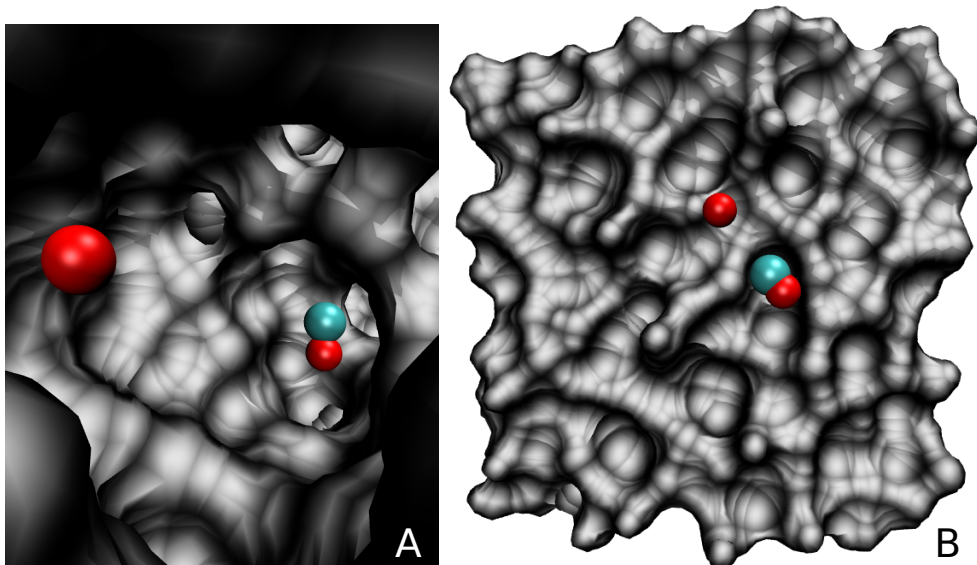


Figure 1: The simulation system for studying the $\text{O}(^1\text{D})+\text{CO}(^1\Sigma^+)\rightarrow\text{CO}_2(^1\Sigma_g^+)$ recombination reaction. Panel A: CO and O trapped inside a cavity of ASW; panel B: CO and O on the top of the ASW surface.

In the following, the coordinates are the CO stretch r , the separation R between the center of mass of CO_A and O_B and θ is the O_ACO_B angle. Initial conditions were generated for a grid of angles θ and separations R and simulations were carried out to obtain initial coordinates and velocities for each of the grid points. With constrained CO and O position, first 750 steps of steepest descent and 100 steps Adopted Basis Newton-Raphson minimization were carried out, followed by 50 ps heating dynamics to 50 K. Then, 100 ps equilibration dynamics was carried out. From each of the runs coordinates and velocities were saved regularly to obtain initial conditions for each combination of angle and distance. Production simulations 500 ps or 6 ns in length were then run from saved coordinates and velocities in the NVE ensemble. Data (energies, coordinates and velocities) were saved every 1000 steps for subsequent analysis.

Water was described by a reparametrized,^{36,37} flexible (Kumagai, Kawamura, Yokokawa - KKY) model³⁸ was used. The typical water modes that couple in the $\sim 2000 \text{ cm}^{-1}$ region relevant in the present work are the water bend (1600 cm^{-1}) and the framework rotation (600 cm^{-1}) as was also found for the vibrational relaxation of cyanide in water.³⁹ To describe $\text{CO}_A + \text{O}_B$ recombination to form CO_2 the Morse-Morse-Harmonic (MMH) parametrization was employed.³⁵ This model treats the two CO bonds with a Morse potential and the OCO bend as a harmonic function. MMH is a computationally efficient model (fitted to MRCI/aug-cc-pVTZ data), which yields results for recombination probabilities on ASW comparable to a more elaborate reproducing kernel Hilbert space (RKHS) representation.^{30,35}

For CO_2 , the partial charges were $q_{\text{O}} = -0.3e$ and $q_{\text{C}} = 0.6e$ with standard van der Waals parameters from CHARMM. These charges are consistent with those obtained from B3LYP/6-31G(d,p) calculations snapshots from the MD simulations with CO_2 adsorbed to a small water cluster $(\text{H}_2\text{O})_{10}$ which yield $q_{\text{C}} = 0.73e$ and $q_{\text{O}} = -0.35e$. This compares with charges of $q_{\text{C}} = 0.22e$ and $q_{\text{O}} = -0.21e$ for the CO molecule and $q_{\text{O}} = -0.1e$ for an oxygen atom adsorbed to $(\text{H}_2\text{O})_{10}$. To assess the dependence of the results on the partial charges used, additional reactive MD simulations using the MMH parametrization were carried out with $q_{\text{O}} = -0.1e$ and $q_{\text{C}} = 0.2e$ (i.e. $q_{\text{CO}} = 0.1e$) and with $q_{\text{O}} = -0.2e$ and $q_{\text{C}} = 0.4e$ (i.e. $q_{\text{CO}} = 0.2e$). In all cases, recombination was found to speed up compared with $q_{\text{CO}} = 0.3e$ and $q_{\text{O}} = -0.3e$ due to the increased mobility of the CO molecule and the O atom on the ASW when reduced partial charges are used.

The main focus of the present work is to study the energy redistribution within the system following recombination of $\text{CO}_A + \text{O}_B$ to form CO_2 . For this, the average total, translational and internal energy of the water molecules is analyzed for recombination on top of and inside ASW. Both, the time scale and amount of energy dissipated into translational and internal degrees of freedom was determined.

3 Results and Discussion

In the following, the energy distribution in the water matrix of the ASW is separately discussed on the ~ 100 ps and on the nanosecond time scale. Next, the energy flow away from the recombination site is analyzed and, finally, the energy redistribution to neighboring water molecules surrounding the recombination site is considered.

3.1 Recombination on the 100 ps time scale

A typical trajectory for $\text{CO}_A + \text{O}_B$ recombination inside the ASW cavity is shown in Figure 2 (left column). Initially, the C- O_B separation is $\sim 6 \text{ \AA}$ (Figure 2A). Within 150 ps recombination takes place and angular distortions lead to exploration of angles $\theta \sim 90^\circ$ (Figure 2B). Relaxation of the angle occurs within the following 50 ps and the CO_2 molecule remains in an internally excited state on much longer time scales, see Figure 2C.³⁵ Concomitantly, the average internal energy of the surrounding water molecules increases by about 10 %, see black, red and green traces in panels D and E of Figure 2. The translational (phononic) modes (green) acquire approximately 1/3 of the additional energy whereas the internal energy (red) increases by the remaining 2/3.

Figure 2 (right column) reports a recombination trajectory on top of ASW. In this case, recombination takes place after ~ 35 ps and wide angular excursions extend out to 100 ps. The amount of energy picked up by the water matrix is larger compared to recombination inside ASW (Panels D and E in figure 2). The average total energy per water molecule increases by close to 20 % and the amount that goes into internal degrees of freedom is considerably larger. For the translational modes, the energy after recombination is comparable to that

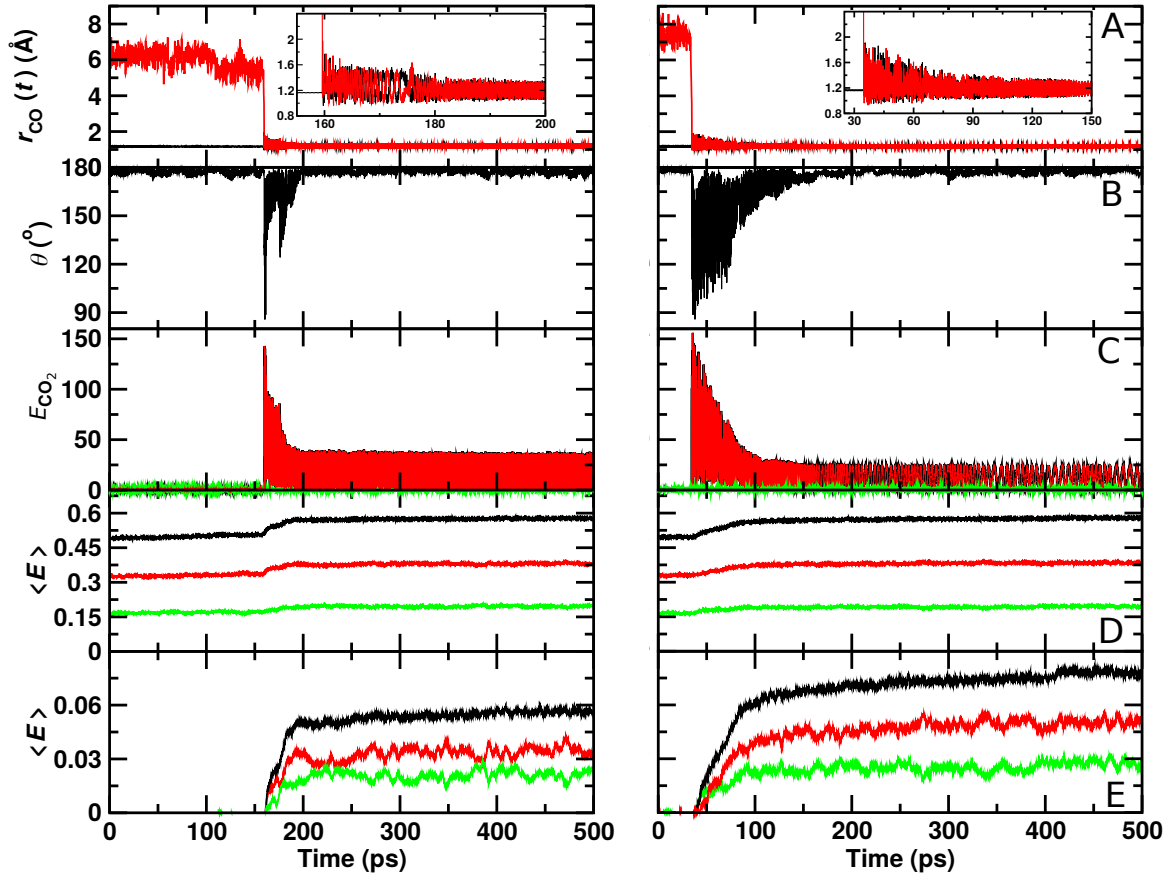


Figure 2: Recombination of $O(^1D) + CO(^1\Sigma^+)$ to form ground state $CO_2(^1\Sigma_g)$ in the ASW cavity (left column) and on top of the ASW surface (right column). Panel A: O_B-CO separation (red) and CO_A separation (black); Panel B: the O-C-O angle θ ; Panels C to E: the average total (black), internal (red), and translational (green) energies for the CO_2 molecule (panel C), the average per water molecule (panel D), and the magnitude of the average per water molecule relative to the energy before recombination (panel E).

for recombination within the cavity.

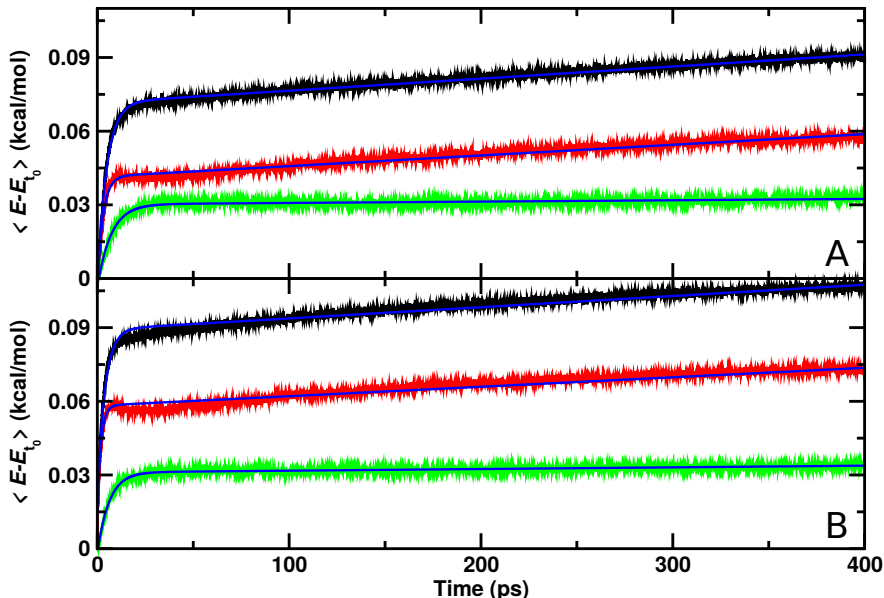


Figure 3: Average total, internal and translational energies for water over 70 independent runs relative to the average before recombination. The time of reaction for all trajectories is shifted to $t = 0$ and defined by the first instance at which $r_{C-O_B} < 1.6$. Panel A: recombination within the ASW cavity. Panel B: recombination for $CO_A + O_B$ on the top of the ASW surface. The blue solid line is a fit to an empirical expression $\epsilon = a_0 e^{-t/a_1} + a_2 t + a_3$, see text.

From a set of 70 recombination trajectories for the reaction within the cavity and on top of the ASW surface, the averaged energy contents in translational, internal and all degrees of freedom of the water molecules were determined (see Figure 3). For this analysis, the time of reaction was set to zero ($t = 0$) to align all reactive trajectories and all energies are reported relative to the averages before recombination. The translational contribution for recombination within and on top of ASW re-equilibrates on the ~ 25 ps time scale after which no change in the phononic degrees of freedom is observed. Contrary to that, the internal degrees of freedom (red traces) show temporal evolution on two time scales: a rapid

phase on the picosecond time scale, followed by a slow, long increase in the internal energies. This is also reflected in the averaged total energy (black).

As for the single trajectories, the amount of energy released from the recombination reaction into the translational degrees of freedom is similar for the reaction inside the cavity and on top of the ASW surface. For the internal degrees of freedom, however, recombination on top of the ASW surface leads on an average increase per water molecule by 0.075 kcal/mol within 400 ps (Figure 3B) compared with 0.06 kcal/mol for the process inside the cavity. Also, there is a characteristic decrease in the internal contribution for recombination on the surface after 15 ps which is even present when averaging over 70 independent runs. This feature is not found for recombination within ASW.

To estimate approximate time scales for the different processes involved, the average energies were fitted to an empirical expression $\epsilon = a_0 e^{-t/a_1} + a_2 t + a_3$ where ϵ is any of the energies considered. Such a functional form was chosen after inspection of the data in Figure 3 and accounts for the rapid initial increase in the three energies together with the slow variation of the internal energy on longer times. This parametrization is not able to model the dip around 15 ps for recombination on top of the surface, though. The time scales a_1 for total, internal, and translational energies are [4.8, 2.9, 7.1] ps for recombination inside the cavity and speed up to [3.9, 1.9, 6.1] ps for the process on the ASW surface. It is of interest to note that the rapid time scale for the internal energy is considerably faster than the kinetics of the translational degrees of freedom for both types of recombinations. The parameter a_2 which describes the slow increase of internal energy has a value of $a_2 = 4.3 \times 10^{-2}$ (kcal/mol)/ns for recombination in the cavity and $a_2 = 3.8 \times 10^{-2}$ (kcal/mol)/ns for the reaction on the surface, and is vanishingly small for the translational energy.

Average internal energies from representative independent runs for recombination inside the

cavity and on top of the ASW surface are shown in Figures S1 and S2. For recombination inside the cavity (Figure S1) the results confirm that the energy content in the internal degrees of freedom increases considerably faster than for the translation. Also, it is found that the amount of energy transferred to translation after recombination is smaller than that partitioned into internal degrees of freedom. For recombination on the ASW surface the same observations are made. In addition, the pronounced maximum after ~ 5 ps is present in all examples shown in Figure S2. To provide a molecularly resolved interpretation of this feature the HOH angle time series $\theta(t)$ was analyzed for a trajectory in which CO+O recombination occurred after 35 ps, see Figure S3. At the time of reaction the water bending angle decreases from its average equilibrium value by $\langle\Delta\theta\rangle \sim 1^\circ$ over the next 70 ps after which it relaxes back to the original value. The signature in the internal energy extends over ~ 30 ps, see Figure S2. Hence, it is possible that changes in the average water geometry following CO+O recombination are responsible for the overshooting and subsequent relaxation of the internal energy for the reaction on the surface. Contrary to that, recombination within the cavity is less constrained by the direct interaction with the water molecules which apparently prevents this particular signature in the internal energy to occur.

3.2 Recombination Dynamics on Longer Time Scales

It is also of interest to analyze the energy redistribution on the multi-nanosecond time scale. Figure 4A demonstrates that the average total kinetic energy per water molecule continuously increases even on the nanosecond time scale. Most of this increase is due to the internal degrees of freedom although the translational component also shows a continuous slow increase on the nanosecond time scale.

The relaxation of the CO₂ internal energy is reported in Figure 4B. Within the first few picoseconds (inset) the internal energy is quenched to ~ 10 kcal/mol after which two re-

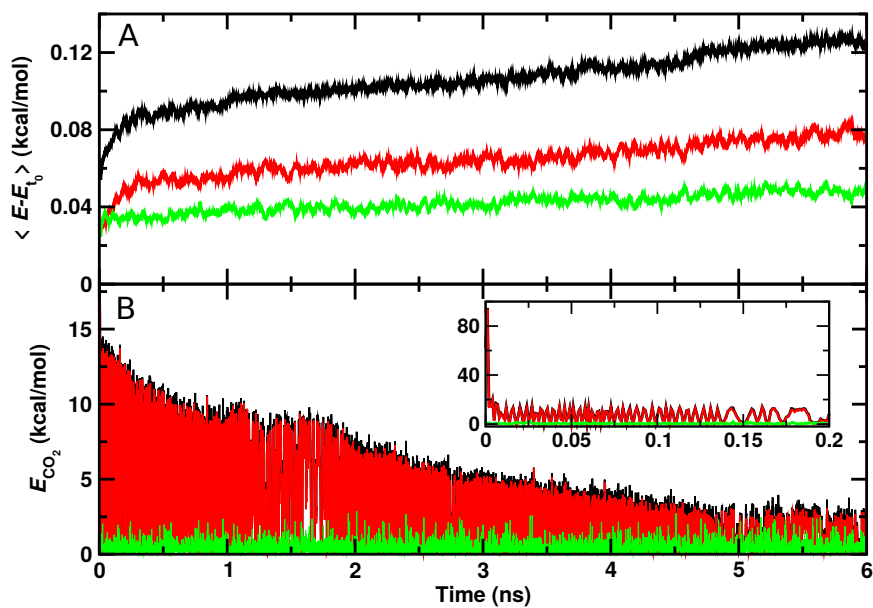


Figure 4: Total (black), internal (red), and translational (green) energies for water molecules (panel A) and for the recombined CO₂ molecule (panel B) from a 6 ns rebinding trajectory on the top of the ASW surface. The time of reaction is shifted to $t = 0$ and defined by the first instance at which $r_{\text{C-O}_B} < 1.6 \text{ \AA}$. CO₂ continues to relax and the energy in the ASW further increases beyond the maximum simulation time of 6 ns after CO₂ recombination.

laxations are observed. A first phase during 1 nanosecond following recombination and a second, slower phase extending out to 6 ns and beyond. By the end of the simulation the average internal energy of the CO₂ molecule has decreased to ~ 2.5 kcal/mol on average. Hence, it is expected that energy transfer to the surrounding water continues but slows down considerably on the 10 ns time scale and longer.

3.3 Energy Migration around the Recombination Site

For a positionally resolved picture of energy flow the simulation system was separated in voxels with dimension $31 \times 1 \times 1 \text{ \AA}^3$. The kinetic energy of all water molecules within one such voxel was averaged along the trajectory and projected onto the (y, z) -plane. Which water molecules belong to a particular voxel was decided based on the water-oxygen atom coordinates. Figure 5A reports the distribution of total kinetic energy distribution before recombination. The recombination site is at $(y = 2, z = 2) \text{ \AA}$ and marked as a large cross. Within the first 5 ps after recombination the kinetic energy of water molecules within $\sim 10 \text{ \AA}$ of the recombination site increases considerably, by up to a factor of 4. Following this, energy redistributes continuously across the entire surface on the 200 ps time scale, see panels C to E.

Certain regions that are initially “cold” (blue) - e.g. the region labelled “I” at $(y = 5, z = -5) \text{ \AA}$ in Figure 5 - warm up as energy transfer from CO₂ to the water molecules occurs. Conversely, other regions remain “cool”, such as region “II” around $(y = 5, z = 5) \text{ \AA}$ for which the color code remains blue until 200 ps. Yet for other regions, such as “III”, the total kinetic energy oscillates between cooler and warmer. It is also instructive to include only the first few ASW layers in this analysis which was done in Figure S4. Here, the voxels have sizes $10 \times 1 \times 1 \text{ \AA}$. For one, the cool regions are more extended before recombination. After recombination energy transfer occurs in a similar fashion as for the full system. However, the warm regions are less extended. This suggests that energy transfer also occurs to a consider-

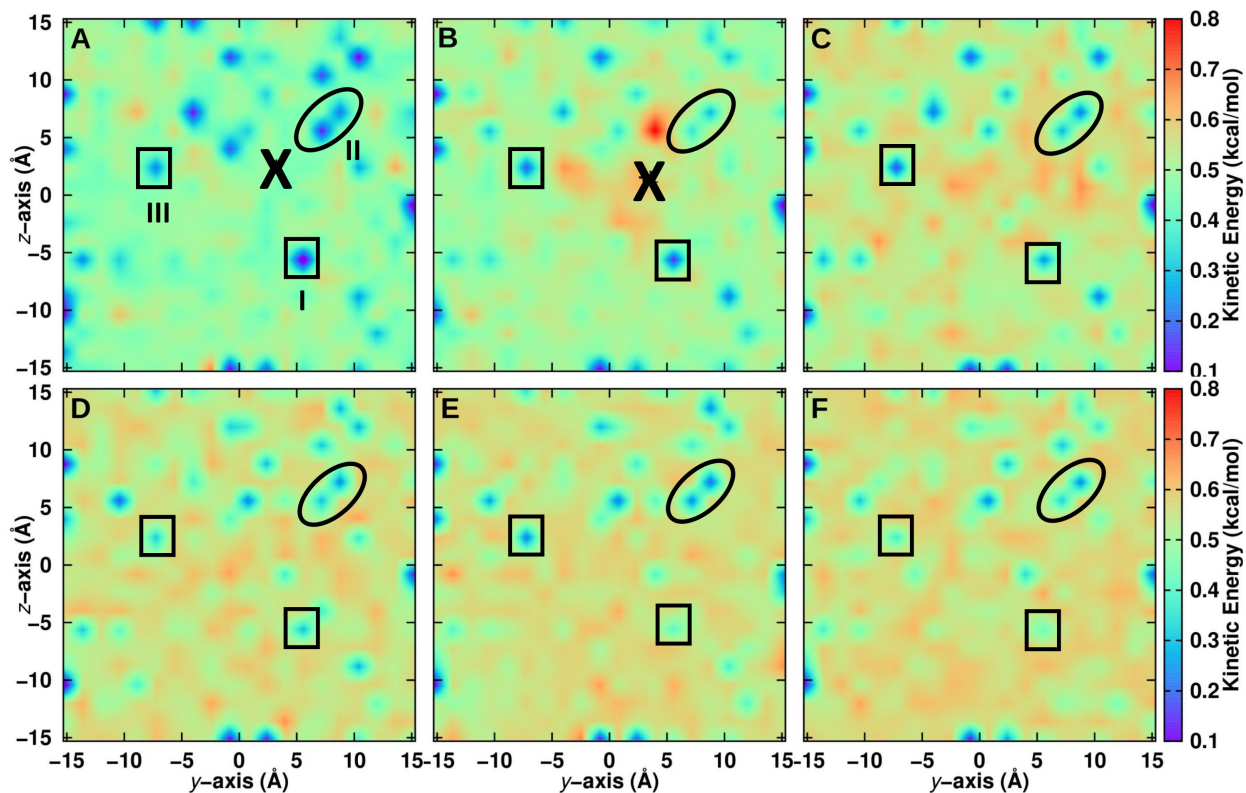


Figure 5: Kinetic energy of water molecules projected onto the (y, z) -plane averaged over 7 independent simulations on the top layer of the ASW surface. Recombination of CO and O takes place at the location labelled with “X”. Before recombination (Panel A: $-5 \leq t \leq 0$ ps) and after recombination (Panel B: $0 \leq t \leq 5$ ps, Panel C: $5 \leq t \leq 10$ ps, Panel D: $10 \leq t \leq 50$ ps, Panel E: $50 \leq t \leq 100$ ps and Panel F: $100 \leq t \leq 200$ ps). The average position of CO is indicated by a large black cross. Noteworthy regions are labelled I to III and surrounded by solid lines. Region I is cool at early times and gradually warms up. Region II remains cool for most of the simulation time and region III alternates between cool and warm. For results within 10 \AA of the surface, see Figure S4.

able extent *into* the bulk rather than across the surface of the ASW even for recombination on top of ASW.

3.4 Energy Flow to Nearby Water Molecules

Finally, individual water molecules in immediate proximity of the recombination site are analyzed. For one trajectory with recombination on the ASW surface the average total, internal, and translational energies for the 5 water molecules closest to the recombination site are reported in Figure 6. During the first 10 ps after recombination the average total kinetic energy increases by up to 0.6 kcal/mol per water molecule. Conversely, the translational energy contribution fluctuates around zero which indicates that the local structure of ASW remains intact and most of the energy flows into internal degrees of freedom.

After this initial increase, cooling takes place with a long-time average of -0.1 kcal/mol per water molecule in the internal degrees of freedom. On the 500 ps no noticeable changes in the translational energy content is observed. For the CO_2 molecule (see Figure 6B) the translational energy remains small throughout the trajectory whereas the internal energy decreases rapidly within the first 5 ps following recombination. Subsequently, slow cooling on the 100 ps to nanosecond time scale takes place as was already found earlier, see Figure 4.

4 Discussion and Conclusion

The present work reports on the energy redistribution across ASW following $\text{O}(^1\text{D})+\text{CO}(^1\Sigma^+)$ recombination to form $\text{CO}_2(^1\Sigma_g^+)$ on the surface and in a cavity. It is found that energy distribution occurs in two phases, one on the picosecond and one on the nanosecond time scale for both locations. Although the time dependence of the processes is similar for the two

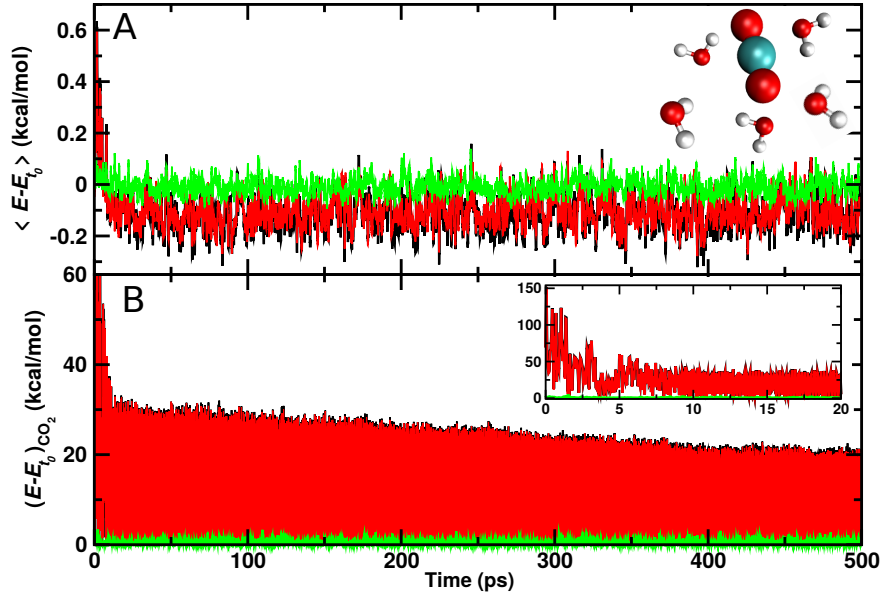


Figure 6: Average total (black), internal (red), and translational (green) energies for 5 water molecules (panel A) closest to the CO_2 , and the CO_2 molecule (panel B) formed from a recombination trajectory on the ASW surface. The time of reaction is shifted to $t = 0$ and defined by the first instance at which $r_{C-O_B} < 1.6$. The initial time scale for energy redistribution from the relaxing CO_2 molecule to internal and translational degrees of freedom of the ASW occurs on the 10 ps time scale with slow gradual relaxation on the ~ 100 ps to ns time scale.

different recombination sites (inside vs. on top), the dynamics differs in a number of ways. Firstly, recombination on the surface leads to excess internal energy on the picosecond time scale which subsequently relaxes and additional energy transfer into water modes occurs on longer time scales. Secondly, recombination within the cavity considered here leads to smaller magnitude ($\sim 15\%$) of energy transferred per water molecule compared with the process on the surface ($\sim 25\%$). Energy relaxation of the CO_2 from recombination on the surface extends over longer times than for the process in the cavity. Finally, heating of the water molecules occurs on the 10 ps time scale following the recombination reaction.

It is of interest to note that - ultimately - energy redistribution in such systems follows quantum mechanical principles. The present results suggest that the local energy generated from $\text{CO}+\text{O}$ recombination is probably sufficient to excite internal modes of individual water molecules surrounding the recombination site. Hence, after $\text{CO}+\text{O}$ recombination the ASW will be in a state characterized by a few internally and vibrationally excited water molecules embedded into a matrix of water molecules in the ground state. Earlier work on a related problem - the vibrational relaxation of a quantum oscillator coupled to oscillators of a biomolecule⁴⁰ - found that using classical mechanics leads to qualitatively correct results compared with a full quantum treatment. For the relaxation times a moderate factor of 2 for the difference between classical and rigorous quantum simulations was reported. Hence, for the present problem it is also expected that similar conclusions apply and that the nonequilibrium relaxation dynamics of individual vibrationally excited water molecules surrounded by vibrationally cold water molecules can be captured qualitatively from using classical dynamics.

In summary, the present work demonstrates that $\text{O}(^1\text{D})+\text{CO}(^1\Sigma^+)$ recombination to form $\text{CO}_2(^1\Sigma_g^+)$ leads to excitation of both, phononic and internal modes of the water molecules that constitute the ASW. The time scales for this are on the pico- and nano-second and lead

to warming the water matrix. Water molecules in direct proximity of the recombination site may become vibrationally excited and the time scale for their relaxation back to the ground state will depend on the coupling to the immediate environment. Full relaxation of the CO₂ molecule is expected to occur on the several 10 to 100 nanosecond time scale.

Acknowledgments

The authors gratefully acknowledge financial support from the Swiss National Science Foundation through grant 200021-117810 and to the NCCR-MUST.

References

- (1) Hagen, W.; Tielens, A.; Greenberg, J. The infrared spectra of amorphous solid water and ice Ic between 10 and 140 K. *Chem. Phys.* **1981**, *56*, 367–379.
- (2) Jenniskens, P.; Blake, D. Structural transitions in amorphous water ice and astrophysical implications. *Science* **1994**, *265*, 753–756.
- (3) Bossa, J. B.; Isokoski, K.; de Valois, M. S.; Linnartz, H. Thermal collapse of porous interstellar ice. *Astron. Astrophys.* **2012**, *545*, A82.
- (4) Bar-Nun, A.; Dror, J.; Kochavi, E.; Laufer, D. Amorphous water ice and its ability to trap gases. *Phys. Rev. B* **1987**, *35*, 2427–2435.
- (5) Oba, Y.; Miyauchi, N.; Hidaka, H.; Chigai, T.; Watanabe, N.; Kouchi, A. Formation of Compact Amorphous H₂O Ice by Codeposition of Hydrogen Atoms with Oxygen Molecules on Grain Surfaces. *Astrophys. J.* **2009**, *701*, 464–470.

- (6) Keane, J.; Tielens, A.; Boogert, A.; Schutte, W.; Whittet, D. Ice absorption features in the 5-8 μm region toward embedded protostars. *Astron. Astrophys.* **2001**, *376*, 254–270.
- (7) Bossa, J.-B.; Isokoski, K.; Paardekooper, D. M.; Bonnin, M.; van der Linden, E. P.; Triemstra, T.; Cazaux, S.; Tielens, A. G. G. M.; Linnartz, H., Porosity measurements of interstellar ice mixtures using optical laser interference and extended effective medium approximations. *Astron. Astrophys.* **2014**, *561*, A136.
- (8) Bossa, J.-B.; Maté, B.; Fransen, C.; Cazaux, S.; Pilling, S.; Rocha, W. R. M.; Ortigoso, J.; Linnartz, H. Porosity and band-strength measurements of multi-phase composite ices. *Astrophys. J.* **2015**, *814*, 47.
- (9) Cazaux, S.; Bossa, J.-B.; Linnartz, H.; Tielens, A. G. G. M., Pore evolution in interstellar ice analogues - Simulating the effects of temperature increase. *Astron. Astrophys.* **2015**, *573*, A16.
- (10) Ioppolo, S.; Cuppen, H. M.; Linnartz, H. Surface formation routes of interstellar molecules: hydrogenation reactions in simple ices. *Rend. Lincei.* **2011**, *22*, 211–224.
- (11) Romanzin, C.; Ioppolo, S.; Cuppen, H. M.; van Dishoeck, E. F.; Linnartz, H. Water formation by surface O_3 hydrogenation. *J. Chem. Phys.* **2011**, *134*, 084504.
- (12) Chaabouni, H.; Minissale, M.; Manicò, G.; Congiu, E.; Noble, J. A.; Baouche, S.; Accolla, M.; Lemaire, J. L.; Pirronello, V.; Dulieu, F. Water formation through $\text{O}_2 + \text{D}$ pathway on cold silicate and amorphous water ice surfaces of interstellar interest. *J. Chem. Phys.* **2012**, *137*, 234706.
- (13) Minissale, M.; Congiu, E.; Baouche, S.; Chaabouni, H.; Moudens, A.; Dulieu, F.; Accolla, M.; Cazaux, S.; Manico, G.; Pirronello, V. Quantum Tunneling of Oxygen Atoms on Very Cold Surfaces. *Phys. Rev. Lett.* **2013**, *111*, 053201.

- (14) Dulieu, F.; Minissale, M.; Bockelée-Morvan, D., Production of O₂ through dismutation of H₂O₂ during water ice desorption: a key to understanding comet O₂ abundances. *Astron. Astrophys.* **2017**, *597*, A56.
- (15) Pezzella, M.; Unke, O. T.; Meuwly, M. Molecular Oxygen Formation in Interstellar Ices Does Not Require Tunneling. *J. Phys. Chem. Lett.* **2018**, *9*, 1822–1826.
- (16) Pezzella, M.; Meuwly, M. O₂ formation in cold environments. *Phys. Chem. Chem. Phys.* **2019**, *21*, 6247–6255.
- (17) Hama, T.; Watanabe, N. Surface Processes on Interstellar Amorphous Solid Water: Adsorption, Diffusion, Tunneling Reactions, and Nuclear-Spin Conversion. *Chem. Rev.* **2013**, *113*, 8783–8839.
- (18) Minissale, M.; Congiu, E.; Manicò, G.; Pirronello, V.; Dulieu, F. CO₂ formation on interstellar dust grains: a detailed study of the barrier of the CO channel. *Astron. Astrophys.* **2013**, *559*, A49.
- (19) Minissale, M.; Moudens, A.; Baouche, S.; Chaabouni, H.; Dulieu, F. Hydrogenation of CO-bearing species on grains: unexpected chemical desorption of CO. *Mon. Not. Roy. Astron. Soc.* **2016**, *458*, 2953–2961.
- (20) Minissale, M.; Fedoseev, G.; Congiu, E.; Ioppolo, S.; Dulieu, F.; Linnartz, H. Solid state chemistry of nitrogen oxides – Part I: surface consumption of NO. *Phys. Chem. Chem. Phys.* **2014**, *16*, 8257–8269.
- (21) Minissale, M.; Congiu, E.; Dulieu, F. Direct measurement of desorption and diffusion energies of O and N atoms physisorbed on amorphous surfaces. *Astron. Astrophys.* **2016**, *585*, A146.
- (22) Minissale, M.; Nguyen, T.; Dulieu, F., Experimental study of the penetration of

- oxygen and deuterium atoms into porous water ice. *Astron. Astrophys.* **2019**, *622*, A148.
- (23) Minissale, M.; Congiu, E.; Manicò, G.; Pirronello, V.; Dulieu, F. CO₂ formation on interstellar dust grains: a detailed study of the barrier of the CO channel. *Astron. Astrophys.* **2013**, *559*, A49.
- (24) Lee, M. W.; Meuwly, M. Diffusion of atomic oxygen relevant to water formation in amorphous interstellar ices. *Faraday Discuss.* **2014**, *168*, 205–222.
- (25) Roser, J. E.; Vidali, G.; Manicò, G.; Pirronello, V. Formation of carbon dioxide by surface reactions on ices in the interstellar medium. *Astrophys. J. Lett.* **2001**, *555*, L61.
- (26) Stief, L. J.; Payne, W. A.; Klemm, R. B. A flash photolysis–resonance fluorescence study of the formation of O(¹D) in the photolysis of water and the reaction of O(¹D) with H₂, Ar, and He-. *J. Chem. Phys.* **1975**, *62*, 4000–4008.
- (27) Garstang, R. Energy levels and transition probabilities in p² and p⁴ configurations. *Mon. Not. R. Astron. Soc.* **1951**, *111*, 115–124.
- (28) Fournier, J.; Deson, J.; Vermeil, C.; Pimentel, G. Fluorescence and thermoluminescence of N₂O, CO, and CO₂ in an argon matrix at low temperature. *J. Chem. Phys.* **1979**, *70*, 5726–5730.
- (29) Ruffle, D. P.; Herbst, E. New models of interstellar gas-grain chemistry - III. Solid CO₂. *Mon. Not. R. Astron. Soc.* **2001**, *324*, 1054–1062.
- (30) Veliz, J. C. S. V.; Koner, D.; Schwilk, M.; Bemish, R. J.; Meuwly, M. The C(³P) + O₂(³Σ_g⁻) ↔ CO₂ ↔ CO(¹Σ⁺) + O(¹D)/O(³P) Reaction: Thermal and Vibrational Relaxation Rates from 15 K to 20000 K. *Phys. Chem. Chem. Phys.* **2021**, *23*, 11251–11263.

- (31) Ghesquière, P.; Mineva, T.; Talbi, D.; Theulé, P.; Noble, J.; Chiavassa, T. Diffusion of molecules in the bulk of a low density amorphous ice from molecular dynamics simulations. *Phys. Chem. Chem. Phys.* **2015**, *17*, 11455–11468.
- (32) Noble, J.; Congiu, E.; Dulieu, F.; Fraser, H. Thermal desorption characteristics of CO, O₂ and CO₂ on non-porous water, crystalline water and silicate surfaces at submonolayer and multilayer coverages. *Mon. Not. R. Astron. Soc.* **2012**, *421*, 768–779.
- (33) Brooks, B.; III, C. B.; Jr, A. M.; Nilsson, L.; Petrella, R.; Roux, B.; Won, Y.; Archontis, G.; Bartels, C.; Boresch, S. et al. CHARMM: the biomolecular simulation program. *J. Comp. Chem.* **2009**, *30*, 1545–614.
- (34) T. Nagy, J. Y. R.; Meuwly, M. Multi-Surface Adiabatic Reactive Molecular Dynamics. *J. Chem. Theo. Comp.* **2014**, *10*, 1366–1375.
- (35) Upadhyay, M.; Pezzella, M.; Meuwly, M. Genesis of Polyatomic Molecules in Dark Clouds: CO₂ Formation on Cold Amorphous Solid Water. *J. Phys. Chem. Lett.* **2021**, *12*, 6781–6787.
- (36) Burnham, C. J.; Li, J. C.; Leslie, M. Molecular Dynamics Calculations for Ice Ih. *J. Phys. Chem. B* **1997**, *101*, 6192–6195.
- (37) Plattner, N.; Meuwly, M. Atomistic Simulations of CO Vibrations in Ices Relevant to Astrochemistry. *ChemPhysChem* **2008**, *9*, 1271–1277.
- (38) Kumagai, N.; Kawamura, K.; Yokokawa, T. An Interatomic Potential Model for H₂O: Applications to Water and Ice Polymorphs. *Mol. Sim.* **1994**, *12*, 177–186.
- (39) Lee, M. W.; Meuwly, M. On the role of nonbonded interactions in vibrational energy relaxation of cyanide in water. *J. Phys. Chem. A* **2011**, *115*, 5053–5061.
- (40) Stock, G. Classical simulation of quantum energy flow in biomolecules. *Phys. Rev. Lett.* **2009**, *102*, 118301.

Supporting Information: Energy Redistribution following CO₂ Formation on Cold Amorphous Solid Water

Meenu Upadhyay and Markus Meuwly*

*Department of Chemistry, University of Basel, Klingelbergstrasse 80 , CH-4056 Basel,
Switzerland.*

E-mail: m.meuwly@unibas.ch

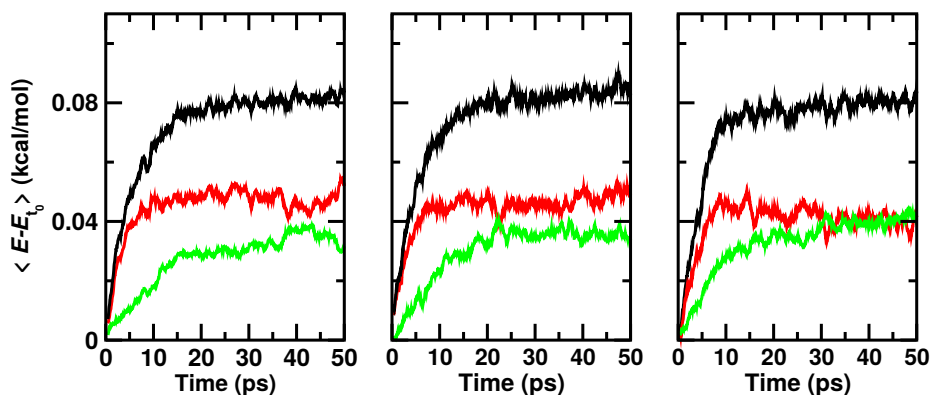


Figure S1: Total (black), internal (red), and translational (green) energies for water molecules from 3 independent simulations inside the ASW cavity. The time of reaction for all is shifted to $t = 0$ and defined by the first instance at which $r_{C-O_B} < 1.6$.

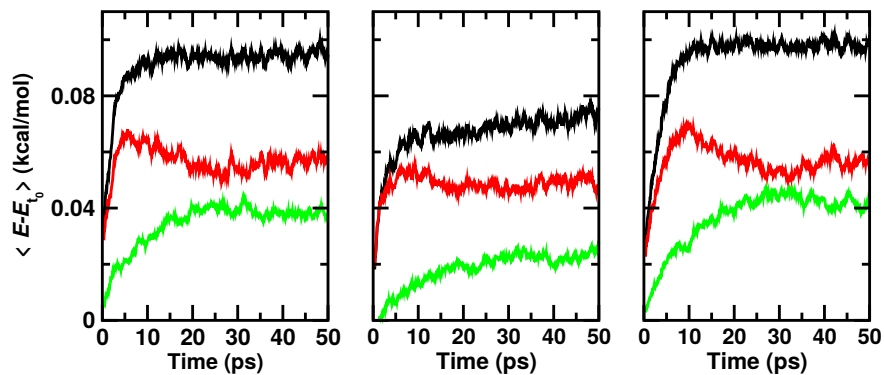


Figure S2: Total (black), internal (red), and translational (green) energies for water molecules from 3 independent simulations on the top of the ASW surface. The time of reaction for all is shifted to $t = 0$ and defined by the first instance at which $r_{C-O_B} < 1.6$.

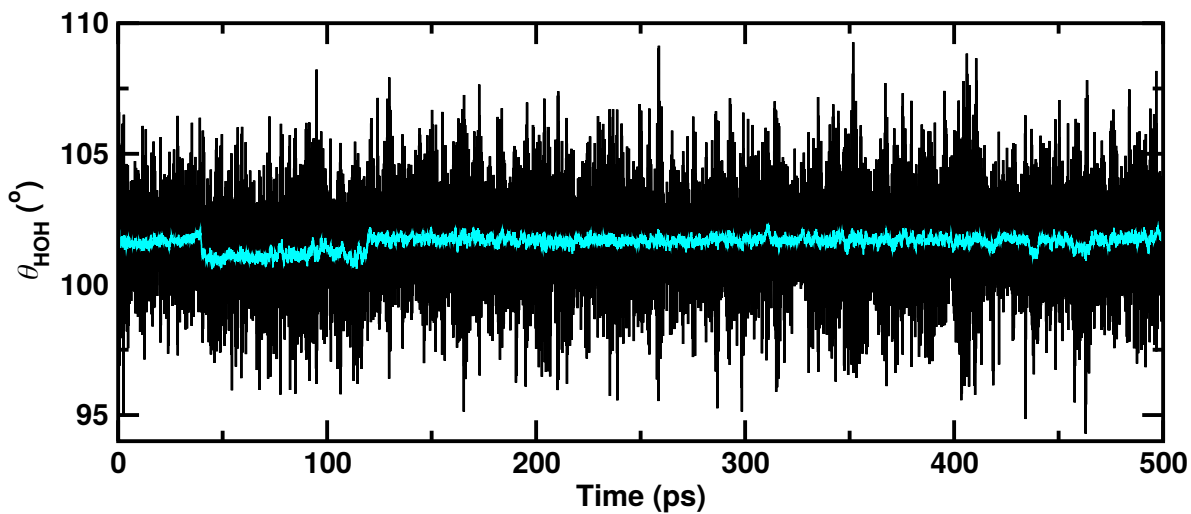


Figure S3: Water bending angle time series for a trajectory with recombination on the surface at $t = 35$ ps.

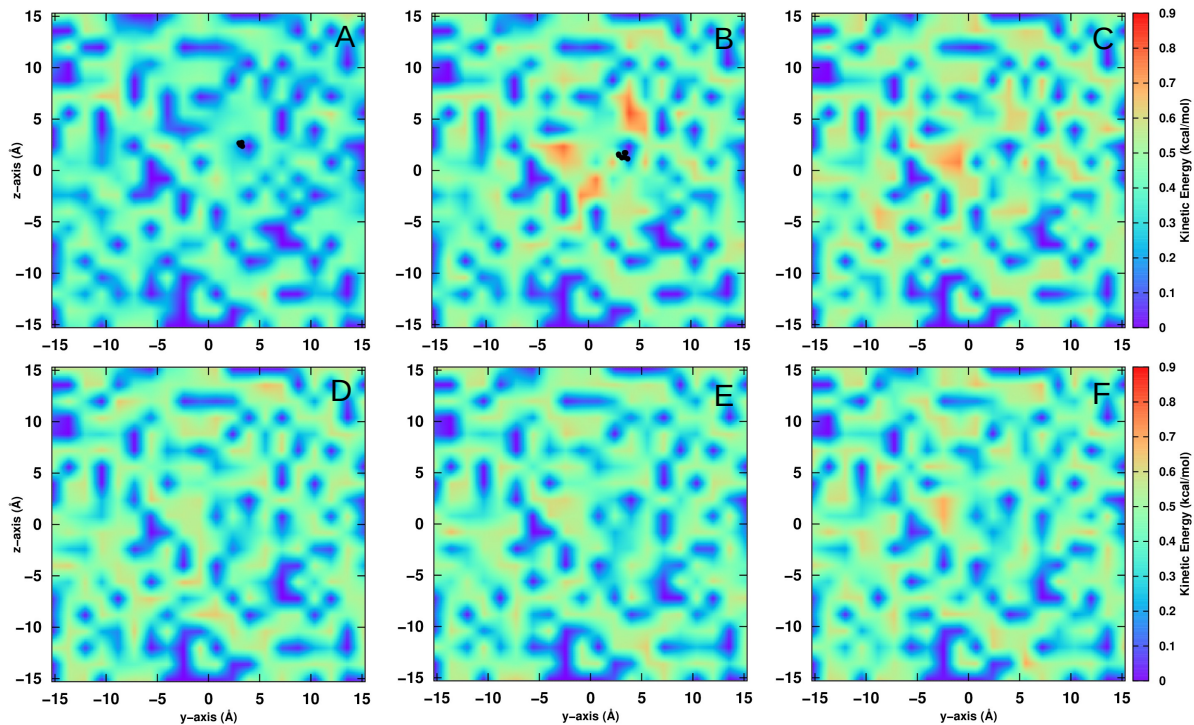


Figure S4: Kinetic energy of water molecules projected onto the (y, z) -plane averaged over 7 independent simulations on the top layer of ASW surface. The kinetic energy is averaged over voxels $10 \times 1 \times 1 \text{ \AA}^3$, i.e. only within 10 \AA of the surface. Here, $t = 0$ is defined as the first instance at which $r_{C-O_B} < 1.6$ and all times are aligned with respect to this reference. Before recombination (Panel A: $-5 \leq t \leq 0$ ps) and after recombination (Panel B: $0 \leq t \leq 5$ ps, Panel C: $5 \leq t \leq 10$ ps, Panel D: $10 \leq t \leq 50$ ps, Panel E: $50 \leq t \leq 100$ ps and Panel F: $100 \leq t \leq 200$ ps). The average position of CO is indicated by black filled circles.